WILEY | Hindawi

Research Article

Rational Design of a Graphene Oxide–Coated Separator for Thermally and Mechanically Stable Li Metal Anode

HeeYoung Lim,[1] **Han Na Na,**[1] **Eun Jung Jung,**[1] **Wook Ahn** [iD],[1,2] **Jong Bae Park** [iD],[3] **John Hong** [iD],[4] **and Young-Woo Lee** [iD][1,2]

[1]*Department of Energy Engineering, Soonchunhyang University, Asan 31538, Republic of Korea*
[2]*Center of Advanced Energy Research, Soonchunhyang University, Asan 31538, Republic of Korea*
[3]*Jeonju Centre, Korea Basic Science Institute, Jeonju 54907, Republic of Korea*
[4]*School of Materials Science and Engineering, Kookmin University, Seoul 02707, Republic of Korea*

Correspondence should be addressed to Jong Bae Park; jbpjb@kbsi.re.kr, John Hong; johnhong@kookmin.ac.kr, and Young-Woo Lee; ywlee@sch.ac.kr

Lithium-ion (Li-ion) batteries are widely used in high-performance energy storage applications because of their high energy density. However, safety concerns related to thermal runaway remain a significant challenge for Li-ion batteries. Electrolyte leakage and dendrite formation can trigger thermal runaway, and these factors typically damage traditional polyethylene (PE) separators. Consequently, these separators struggle under extreme conditions and fail to control dendrite growth. In this study, we proposed a solution by coating PE separators with graphene oxide (GO) layers. GO, as a ceramic material, provides superior thermal and mechanical stability compared with polymers. Moreover, GO-coated PE separators (GO-S) do not compromise the advantages of PE separators and effectively manage dendrite growth. In this study, the as-prepared GO-S exhibits excellent electrochemical properties in terms of high ionic conductivity, suppression of Li dendrite growth during charge/discharge process, and long-term cyclability for 7,000 h (3,500 cycles) as well as high thermal stability even after heat treatment of 100°C. Thus, we expect that this research can highlight the potential application of functionalized GO sheets in addressing the thermal and mechanical limitations of polymer-based separators, thereby enhancing the safety and reliability of Li-ion batteries.

1. Introduction

Recent advancements in modern techniques have been strongly driven by rapid progress in energy storage and generation systems [1–5]. In particular, most energy storage systems use secondary electrochemical energy storage devices such as lithium-ion (Li-ion) batteries [6–8]. These batteries can be used in a wide array of devices, from wearables and smartphones to electric bikes, electric cars, and stationary energy storage units. At present, the battery market focuses on expanding the applicability of Li batteries by developing varieties with high capacity, lightweight construction, and miniaturization. However, despite these technical advancements, serious thermal and fire issues arising from internal thermal runaway continue to raise questions about the stability of Li batteries [9–12]. Several external and internal factors can contribute to the onset of this internal thermal runaway [13–15]. For example, electrolyte leakage and decomposition can be triggered by external factors such as pressure and temperature fluctuations, thereby degrading the performance and safety of the battery [16, 17]. In addition, the uneven deposition of Li during the charge–discharge process can result in the formation of Li dendrites, which pose a significant problem as they can lead to internal

short circuits within the battery [18–20]. Therefore, the use of mechanically and thermally stable separators can minimize the external and internal factors that contribute to thermal runaway.

Conventional polyethylene- (PE-) based separators have many advantages, including high ionic conductivity, flexibility, and ease of fabrication [21, 22]. However, these polymer-based separators encounter challenges under thermal runaway conditions [23–25]. In particular, they struggle to handle internal heat that exceeds 100°C and begin to decompose, which further contributes to short circuits between the anode and cathode. In addition, they are ineffective at blocking and controlling the morphology of dendrites because of their polymeric mechanical properties [26, 27]. In some cases, these protruding dendrites can tear through the separator sheets, leading to malfunctions. Therefore, developing new material candidates and fabricating corresponding separators that retain the advantages of polymer-based separators while addressing their disadvantages are crucial for improving the mechanical and thermal stability as well as ensuring the overall reliability of Li-ion batteries.

In this study, we reported that graphene oxide (GO) coating layers can enhance the intrinsic mechanical and thermal stability of PE-based separators. As ceramic-based materials, GO coating layers provide superior thermal, mechanical, and chemical stability compared with polymers, thereby compensating for the weaknesses of PE-based separators. To improve flexibility and ionic conductivity, the GO samples were synthesized by treating raw graphite with strong oxidizing agents, a process commonly known as Hummers' method. This treatment introduced numerous hydroxyl and epoxy groups on the surface of GO, thereby enhancing its absorptivity for lithium electrolytes while also imparting insulating properties. Furthermore, the functionalized groups on GO are known to improve the wettability of the separator to the electrolyte, thus facilitating additional pathways for lithium-ion transfer [28–44]. In addition, when used as a coating shell on the PE-based separator, the applied GO coating layers do not compromise the advantages of PE-based polymer separators from Li dendrite growth formed during the Li charge/discharge process. Consequently, cells equipped with the GO-coated polymer separator (GO-S) exhibit superior electrochemical performance compared with those equipped with pure PE-based polymer separators (PE-S). In symmetric Li/Li metal cells featuring GO-S, a stable electrochemical plating/stripping cycling is observed for over 7,000 h (3,500 cycles), maintaining a constant overpotential at a capacitance of 0.1 mAh cm^{-2} and a current density of 0.1 mA cm^{-2}. By contrast, cells with PE-S exhibit an increased overpotential and unstable electrochemical plating/stripping behavior, indicating that GO-S can effectively control the morphology of protruding dendrites on the Li anode. Moreover, full cells featuring lithium titanate (LTO) as the cathode and Li metal as the anode (LTO//Li) with GO-S exhibit good rate retention and cycling stability even after aging for 1 h at 100°C. Therefore, the use of functionalized GO sheets as the coating layer can practically and effectively address the thermal and mechanical limitations of polymer-based separators.

2. Materials and Methods

2.1. Preparation of GO-S.
We synthesized GO using modified Hummers' method to prepare GO-S with thickness control. To prepare the GO solution, GO was added to isopropyl alcohol (IPA), and the mixture was stirred. Before the GO coating, sonication for more than 10 min was performed for stable dispersion. This dispersion was then vacuum filtered through a PE separator to generate GO-S.

2.2. Characterization of GO-S.
The sample morphology and surface were observed using field-emission scanning electron microscopy (FE-SEM, Hitachi S-4800, Japan). X-ray diffraction (XRD, Miniflex600 (Rigaku, Tokyo, Japan)) equipped with Cu Kα radiation (40 kV, 15 mA) was performed to analyze the crystal structure of the materials. X-ray photoelectron spectroscopy (XPS, k-alpha+, Thermo Scientific) was used to characterize the chemical state and composition of the samples. Raman spectroscopy (LabRAM HR-800, HORIBA JOBIN YVON, France) equipped with a 514 nm laser was used for the analysis. The contact angle of the electrolyte on the separators was measured in air at room temperature using the sessile drop method equipped with a contact angle meter (DSA25S, KRUSS). The electrolyte uptake by the separators was calculated using the following equation [45, 46]:

$$\text{Uptake} = \frac{W - W_0}{W_0}, \qquad (1)$$

where W_0 and W are the weights of the separator before and after soaking in the 1M LiPF$_6$ (EC : EMC = 1 : 1) electrolyte.

2.3. Electrochemical Measurements of the As-Prepared Separators.
The ionic conductivity of GO-S was measured using electrochemical impedance spectra (EIS) in the frequency range of 100 kHz–0.1 Hz by assembling the electrolyte between two stainless steels. The temperature-dependent ionic conductivity was tested at room temperature. The ionic conductivity of GO-S was calculated by using the following equation [47, 48]:

$$\sigma = \frac{L}{R_b \cdot S}, \qquad (2)$$

where R_b (Ω) is the resistance of the composite electrolytes, L is the thickness (cm), and S is the active area (cm^2) of the GO-based and commercial separator. Electrochemical measurements were conducted using symmetrical and asymmetrical cell configurations involving symmetric Li//Li, asymmetric Li//Li$_4$Ti$_5$O$_{12}$ (LTO), and Li//LiFePO$_4$ (LFP) cells as well as CR2032-type coin cells. The galvanostatic charge/discharge (GCD) of symmetric Li/Li cells was measured at current densities of 1 mA cm^{-2} and 0.01 mA cm^{-2}, respectively. For asymmetric Li//LTO or Li//LFP cells, the LTO or LFP electrodes were produced from mixed slurry with 80 wt% LTO or LFP as the active material, 10 wt% carbon black as a conducting material, and 10 wt% polyvinylidene fluoride as a binder dispersed in N-methylpyrrolidone. The slurry was cast onto the Cu or Al foil (20 μm) and dried at 80°C for 12 h under vacuum.
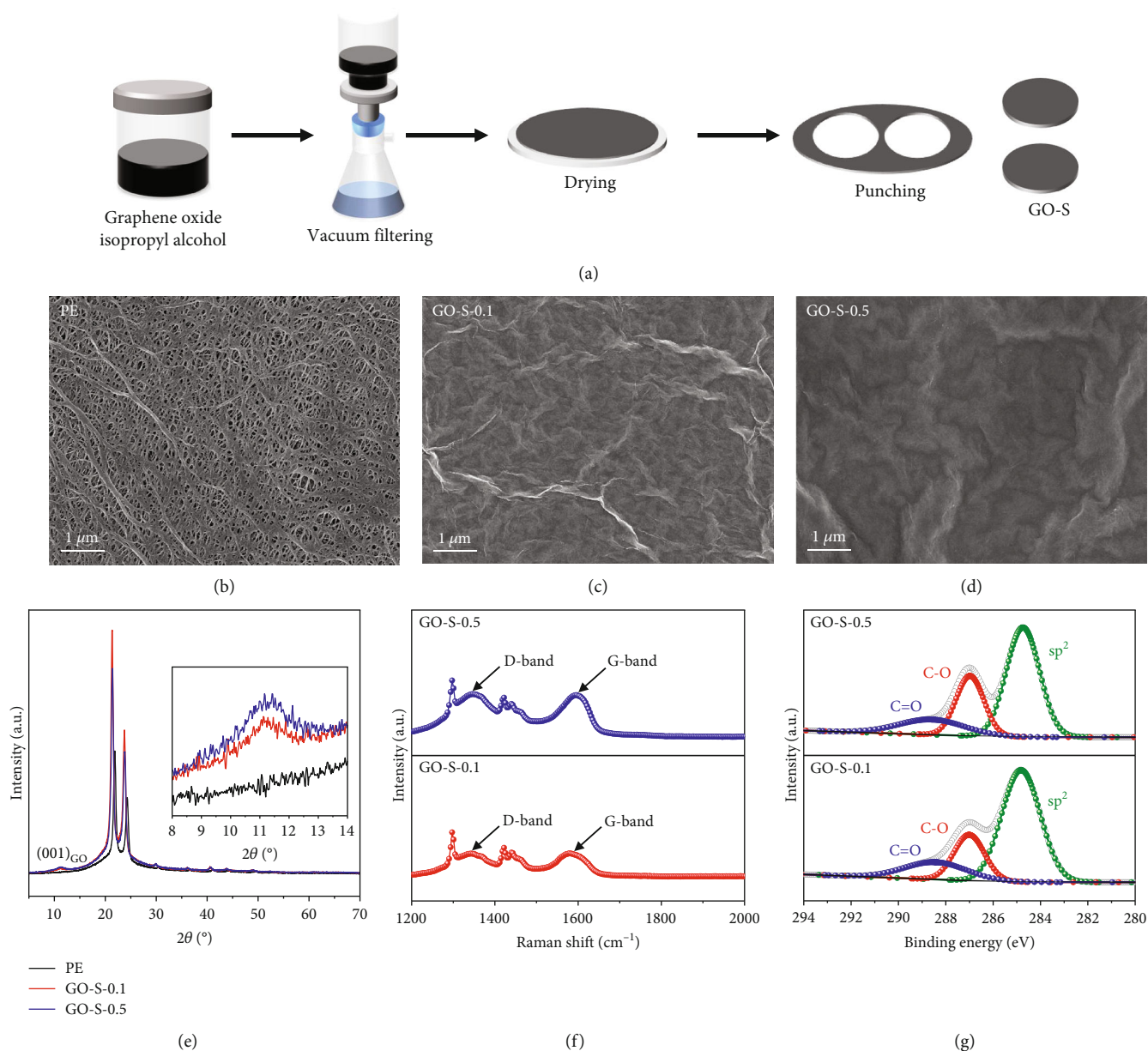
(a)

(b)

(c)

(d)

(e)

(f)

(g)

FIGURE 1: (a) Preparation of graphene oxide-based separator. SEM images of separator (b) PE, (c) GO-S-0.1, and (d) GO-S-0.5. (e) XRD spectra of PE, GO-S-0.1, and GO-S-0.5. (f) Raman spectra of GO-S-0.1 and GO-S-0.5. (g) XPS patterns of GO-S-0.1 and GO-S-0.5.

Finally, the foil was cut into Φ13 mm disks. The coin cells were fabricated in an argon-filled glove box with Li anode metal, LTO or LFP cathode, and GO-S (or PE-S). Electrochemical tests were conducted using a WonATech battery tester (WBCS3000Le).

3. Results and Discussion

3.1. Preparation and Characterization of GO-S. First, GO solution was synthesized from graphite powder (Graphene Supermarket, Ronkonkoma, NY, USA) using the modified Hummers' method. The GO solution dispersed in the IPA was vacuum filtered through a PE separator (denoted as GO-S). During filtration, the volume of GO (either 0.1 mL or 0.5 mL) was controlled to regulate the thickness of the GO layer. Following appropriate drying procedures, GO-S was carefully punched to fit the size of a 2032 coin cell (Figure 1(a)). The physical and chemical properties of the PE membrane after filtration with 0.1 mL (GO-S-0.1) and 0.5 mL (GO-S-0.5) of GO solution were analyzed using SEM, XRD, Raman spectroscopy, and XPS. As shown in Figure 1(b), the surface of the commercially sourced pure PE separator was composed of fiber-woven structures with a number of pores. When 0.1 mL of GO is filtered and subsequently deposited onto the PE separator, most of the pores are fully filled with GO because of its large lateral size, giving the surface a nanosheet-like structure (Figure 1(c)). In addition, when 0.5 mL of GO is used, bulky sheet structures can be observed (Figure 1(d)) because of a thick layer of GO deposited onto the PE membrane. The estimated thickness

of PE-S, GO-S-0.1, and GO-S-0.5 is $10\,\mu m$, $10.6\,\mu m$, and $11.3\,\mu m$, respectively (Figure S1). The thickness slightly increased with the increased volume of GO in filtration solution. XRD analysis of the samples reveals distinct peaks at 2θ angles of $21°$ and $24°$, which can be attributed to the PE membrane [49]. Furthermore, an additional minor XRD peak at a 2θ angle of approximately $11°$ corresponds to the (001) plane of GO (Figure 1(e)), confirming the presence of GO layers on the PE membrane [50]. Figure 1(f) presents the Raman spectra of GO-S-0.1 and GO-S-0.5. Two representative carbon peaks are observed, a slight broadening of the D-band and a G-peak at 1350 and $1590\,cm-1$, respectively, which indicate the presence of oxidized functional groups, including epoxy, hydroxyl, and/or carbonyl groups, on GO [51, 52]. The large number of these functional groups indicates less sp2 bonding on the edge and basal plane of GO, resulting in a relatively high intensity of the D-band. Furthermore, based on the XPS results, the XPS spectra of C 1s for GO-S can be deconvoluted into three binding peaks: C–C bonding at $284\,eV$, C–O bonding at $286\,eV$, and C=O bonding at $288\,eV$ (Figure 1(g)) [53, 54]. Given the high level of functionalized groups and increased thickness, the XPS spectra of GO-S-0.5 show high-intensity peaks originating from the functional groups (at 284 and $286\,eV$) compared with GO-S-0.1, and the ratio of functional groups for GO-S-0.5 is 42.3%.

As shown in Figure 2(a), the surface polarity of GO-S was evaluated through contact angle measurements using a $1.0\,M$ $LiPF_6$ (EC:EMC) solution. The surface of GO-S-0.5 is more favorable than that of GO-S-0.1 and PE, with the contact angle on GO-S-0.5 measuring only $7.9°$. By contrast, the contact angles for GO-S-0.1 and PE stabilize at $10.1°$ and $43.5°$, respectively. The difference in contact angles indicates that the GO-coated layers on the PE membrane enhance surface wettability. Lower contact angles indicate better wettability, which is crucial for electrolyte interactions in Li-ion batteries. Figure 2(b) displays the temperature endurance test of PE and GO-S-0.1, with heat applied ranging from $50°C$ to $200°C$ in a thermal oven. After heat treatment, the surfaces of both samples were observed using optical microscopy. The PE-S began to shrink at $100°C$ and started to decompose at $150°C$, with 80% of its volume lost after reaching $200°C$. By contrast, GO-S-0.1 demonstrated high thermal stability, as the original area and surface structure were well maintained even at $200°C$. Therefore, the GO-coated layers enhance the thermal stability of the inner PE-S, indicating that the GO layers can be a good candidate for the surface protection layer on PE-S. Moreover, the electrolyte uptake of PE-S, GO-S-0.1, and GO-S-0.5 was tested after 1 h of impregnation in a $1.0\,M$ LiPF6 (EC:EMC) solution (Figure 2(c)). The electrolyte uptake for PE-S, GO-S-0.1, and GO-S-0.5 was 330%, 400%, and 450%, respectively. This finding indicates that the large number of functionalized groups on GO-S contributes to the high impregnation ratio. In addition, the ionic conductivities of PE-S, GO-S-0.1, and GO-S-0.5 were evaluated using the bulk resistance values, as determined from the EIS results (Figure 2(d)). The bulk resistances of PE-S, GO-S-0.1, and GO-S-0.5 were calculated to be $2.18\,\Omega$, $1.83\,\Omega$, and $2.75\,\Omega$,

respectively. Based on the impregnation and EIS tests, compared with the impregnation results, GO-S-0.1 showed the lowest bulk resistance compared with GO-S-0.5, indicating faster charge carrier and Li-ion diffusion in the GO-S-0.1 sample. These results indicate that the excessive number of functional groups and increased layer thickness from GO on the PE membrane can decrease the overall electrochemical ion diffusivity. Finally, Figure 2(e) shows the calculated ionic conductivity values for PE-S, GO-S-0.1, and GO-S-0.5. The highest ionic conductivity of GO-S-0.1 would be electrochemically favorable when used as a separator in Li-ion battery cells. Furthermore, consistent with the results of the ionic conductivity results, GO-S-0.1 (0.89) demonstrated a higher Li-ion transference number compared to PE-S (0.84), indicating improved Li diffusion kinetics (Figure S2).

3.2. Electrochemical Performances of GO-S. Symmetric Li/Li cells were used to evaluate the electrochemical performance of Li anode batteries using GO-S-0.1. These cells were used to investigate the galvanostatic Li plating/stripping behavior, overpotential, and corresponding electrochemical behavior at a current density of $1\,mA\,cm^{-2}$ and capacity of $1\,mAh$ cm^{-2} (Figure 3 and S3). As shown in Figures 3(a)–3(c), the overpotential windows for all cells, including those with PE-S, GO-S-0.1, and GO-S-0.5, exhibited similar fluctuations during the initial cycles. These fluctuations are attributed to the side reactions on the Li foil, SEI formation, and inconsistent Li plating/striping behavior during the initial cycles. However, after reaching the stabilization point, the Li plating/striping curves of the Li/Li cells demonstrate relatively small and stable overpotential ranges compared with those observed at the beginning of the charge/discharge cycles. However, for cells with PE-S, the overpotential begins to fluctuate again, ranging from $-1.0\,V$ to $1.0\,V$, after $400\,h$ (Figure 3(a)). By contrast, cells with GO-S-0.1 or GO-S-0.5 continued to display a relatively small overpotential window even after cycling for $600\,h$ (Figures 3(b) and 3(c)). This high overpotential fluctuation in cells with PE-S indicates that the use of PE-S is ineffective at suppressing dendrite growth, modulating morphology, and managing dead Li during Li plating/striping cycling compared with cells with GO-S. Therefore, the use of GO coating layers on the PE membrane provides great mechanical stability and ensures high ion diffusivity from GO, effectively alleviating problems related to dendrites and dead Li. Figures 3(d)–3(g) display the Li plating/striping curves of cells with PE-S, GO-S-0.1, and GO-S-0.5 after $440\,h$ of cycling at a current density of $1\,mA\,cm^{-2}$. Moreover, for cells with PE-S, the overpotential of Li plating/striping behavior continuously increases after each cycle. By contrast, cells with GO-S-0.1 or GO-S-0.5 maintained relatively constant overpotential windows, indicating stable Li plating/striping behavior. Figure 3(g) demonstrates that cells with GO-S-0.1 exhibit the smallest overpotential window compared with those with PE-S and GO-S-0.5. The estimated overall overpotential for cells with GO-S-0.1 is 0.34 V, which is smaller than that of cells with PE-S or GO-S-0.5, accounting for 0.5 and 0.43 V, respectively (Figure 3(h)). The stable overpotential operation and values exhibited by cells with GO-S-0.1 are consistent with the physical and
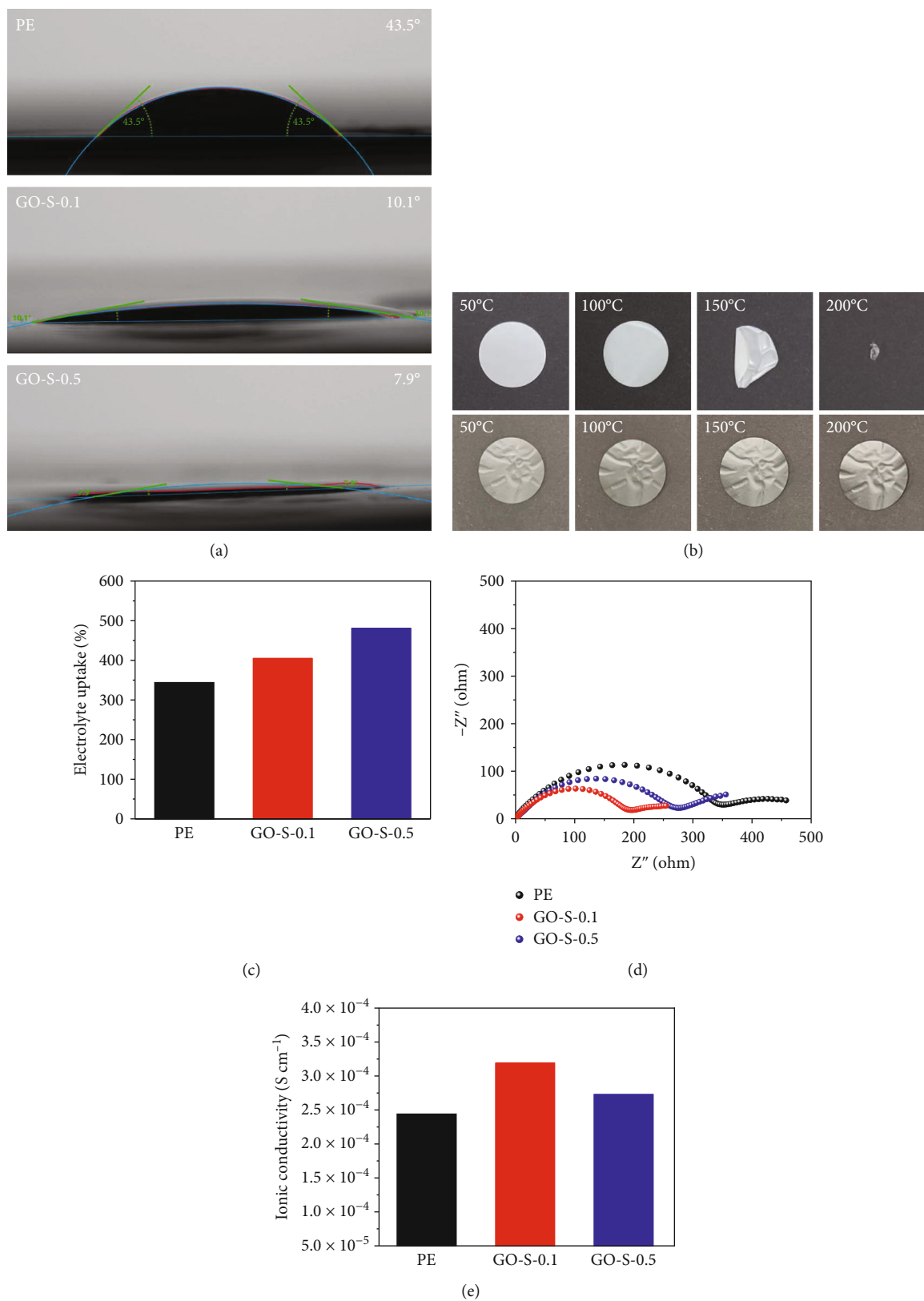
FIGURE 2: (a) Contact angles of liquid electrolyte on the surface of PE, GO-S-0.1, and GO-S-0.5. (b) Thermal stability tests of PE and GO-S. (c) Electrolyte uptake tests of PE, GO-S-0.1, and GO-S-0.5. (d) Electrochemical impedance spectra of PE, GO-S-0.1, and GO-S-0.5. (e) The ionic conductivity of PE, GO-S-0.1, and GO-S-0.5.
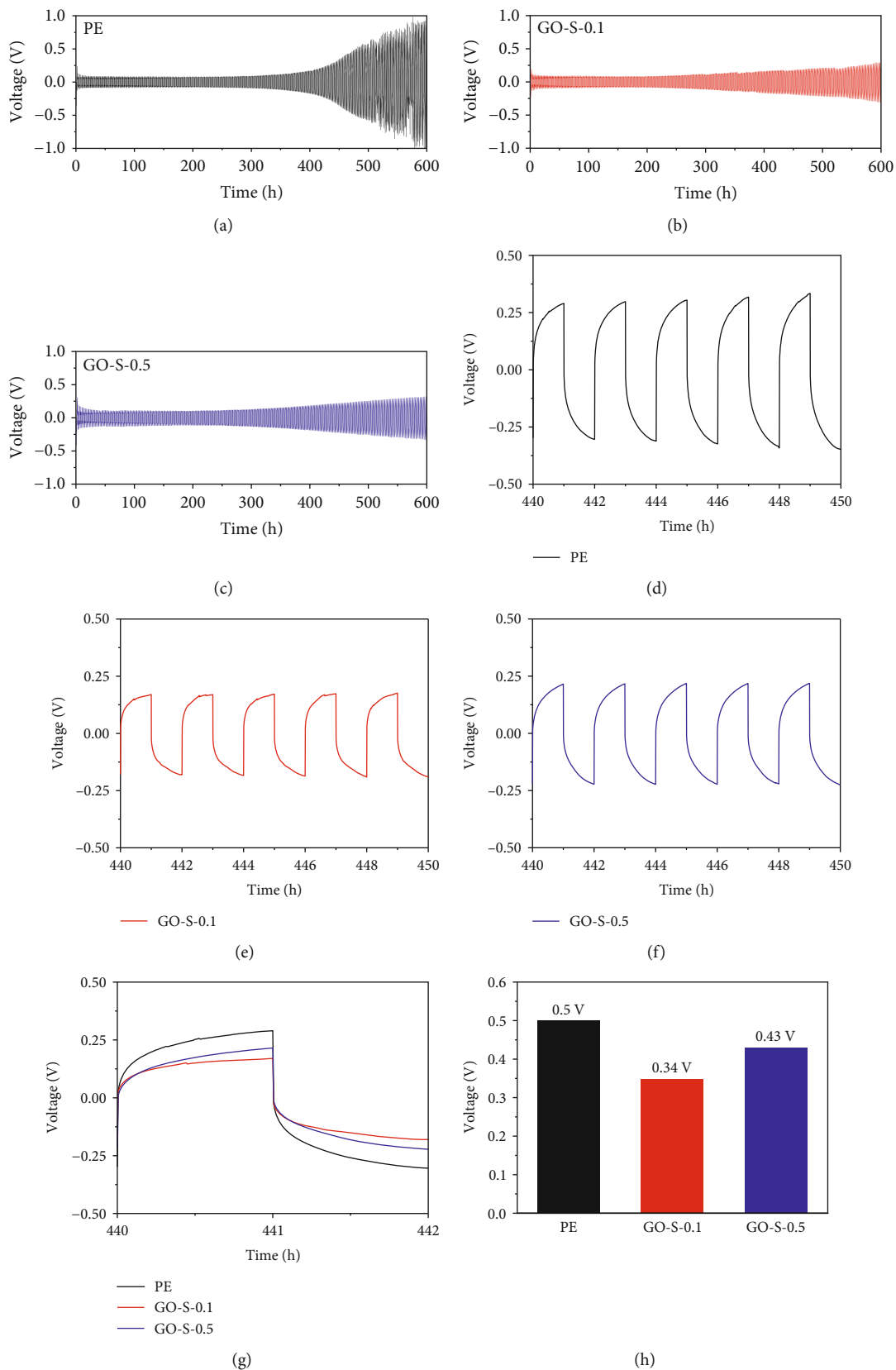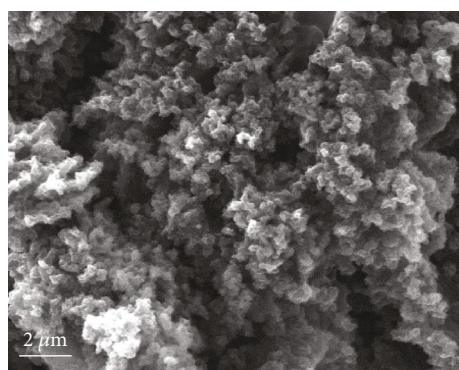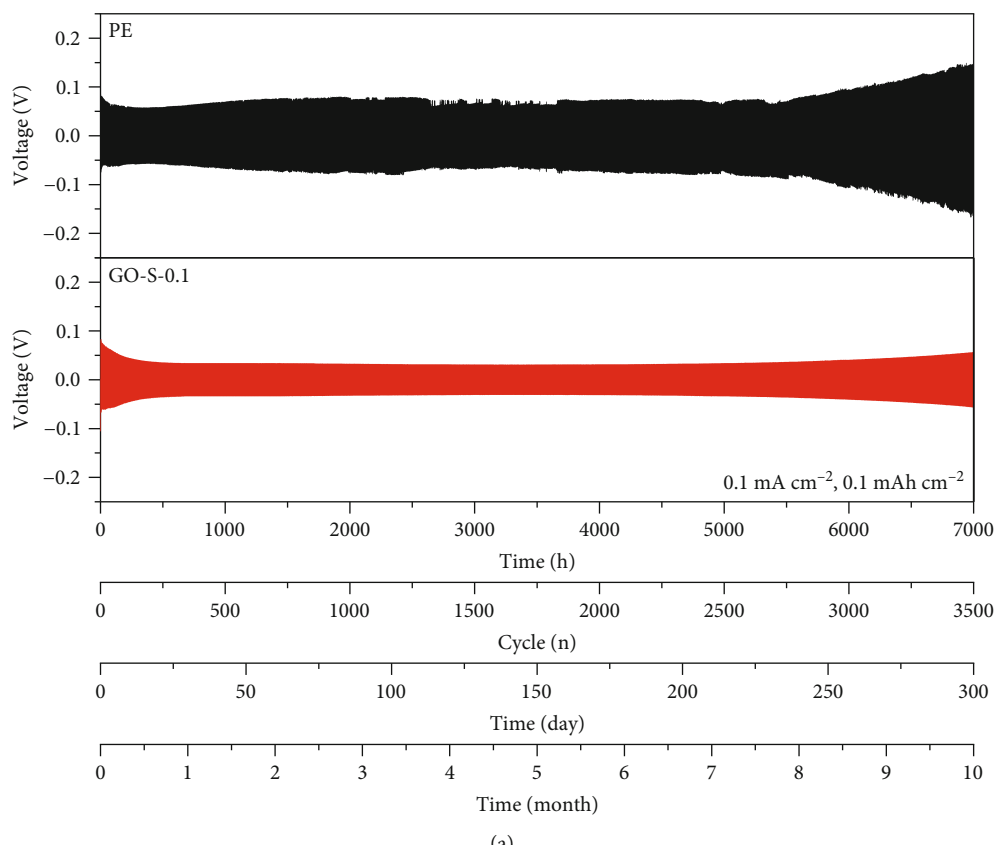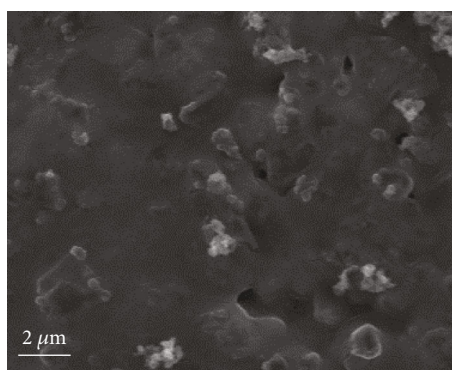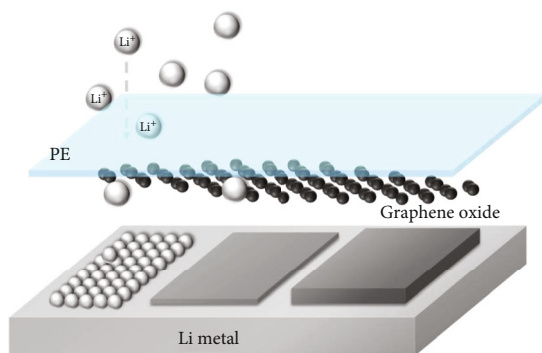
FIGURE 3: Electrochemical performance of (a) Li/PE/Li, (b) Li/GO-S-0.1/Li, and (c) Li/GO-S-0.5/Li cells at the current density of 1 mAh cm^{-2} for 600 h. Li plating/striping curves of Li/PE/Li and Li/GO-S/Li cells from 440 h to 450 h for (d) PE, (e) GO-S-0.1, and (f) GO-S-0.5. (g, h) Overpotential profiles from 440 h to 442 h for PE, GO-S-0.1, and GO-S-0.5.

(a)

(b)

(c)

(d)

FIGURE 4: (a) Long-term electrochemical performance of Li/PE/Li and Li/GO-S-0.1/Li cells at the current density of 0.1 mA cm^{-2} for 7,000 h. SEM images of Li metal surface in Li//Li cells with (b) PE and (c) GO-S-0.1. (d) Scheme characterization of cycled Li dendrite formation in symmetric cells with GO-S and PE.
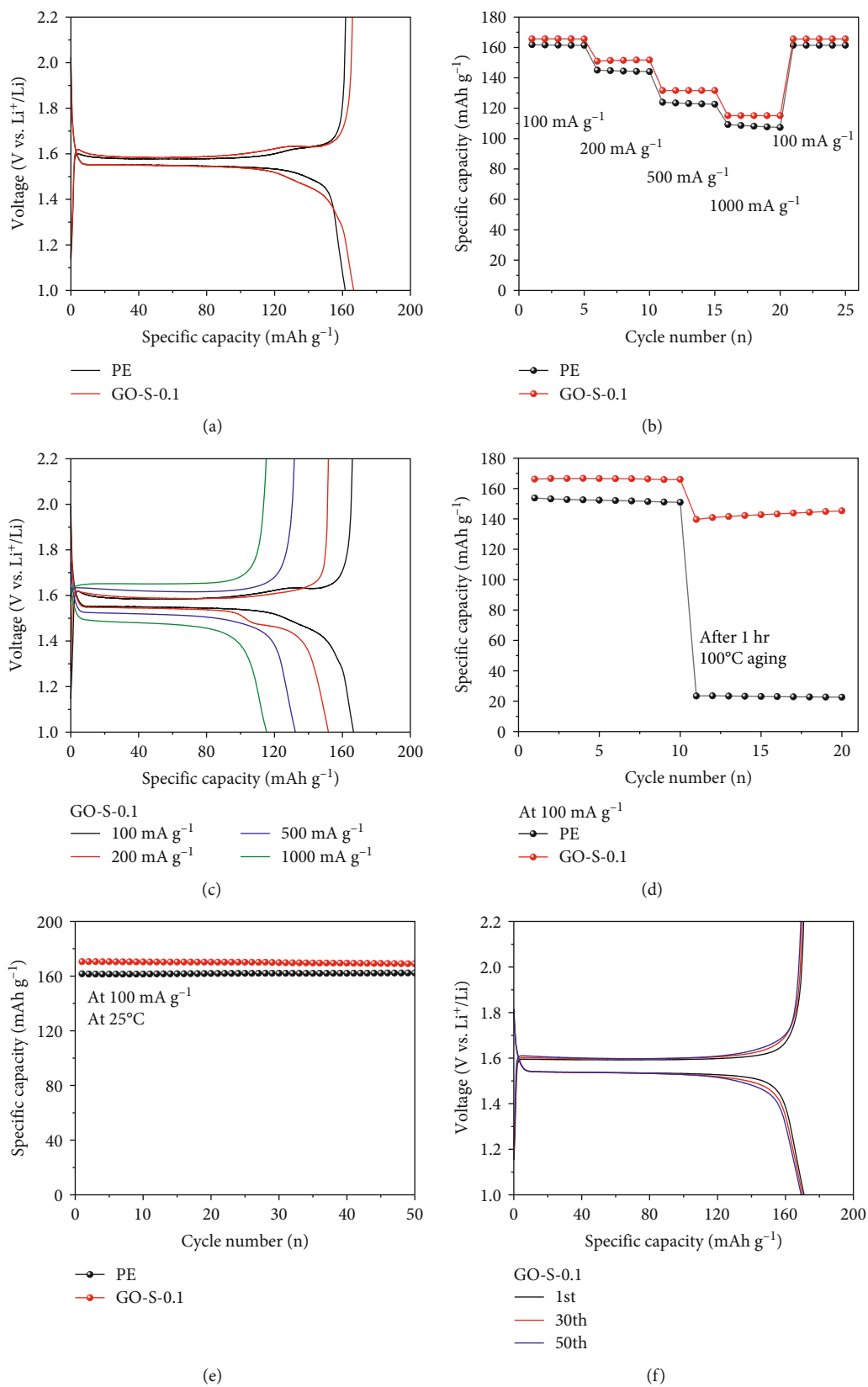
Figure 5: (a) Galvanostatic charge-discharge curves of Li/PE/LTO and Li/GO-S-0.1/LTO cells at 100 mA g⁻¹. (b) Rate capability of Li/PE/LTO and Li/GO-S-0.1/LTO cells under different rate at 25°C. (c) Galvanostatic charge-discharge curves of Li/GO-S-0.1/LTO at various current densities. (d) Thermal test of Li/PE/LTO and Li/GO-S-0.1/LTO cells after 100°C, 1 h aging. (e) Cycling performance of Li/PE/LTO and Li/GO-S-0.1/LTO cells at 100 mA g⁻¹. (f) Galvanostatic charge-discharge curves of Li/GO-S-0.1/LTO cell at different cycles.

electrochemical features indicated in Figure 2, indicating superior electrochemical and mechanical stability for GO-S-0.1.

In addition, to demonstrate the ultralong cyclability and stability of Li anode batteries based on GO-S, we evaluated the Li plating/striping behavior of cells with PE-S and GO-S-0.1 during 7,000 h of cycling, which is equivalent to 3,500 cycles, 300 days, and 10 months, at a current density of 0.1 mA cm^{-2} and a capacity of 1 mAh cm^{-2}. Similar to the electrochemical results measured at a current density of 0.1 mA cm^{-2}, the excellent cycling stability of cells with GO-S-0.1 is evidenced by the small and stable overpotential windows observed after 7,000 h of cycling. After cycling, the surface of the Li anode was examined to assess the morphology of the Li dendrites. On the Li anode treated with PE-S, protruding and mossy Li dendrites were observed (Figure 4(b)). By contrast, when using GO-S-0.1, relatively uniform and flat Li dendrites were found to have grown on the Li anode (Figure 4). Furthermore, after the GO-S-0.1 separator encountered the Li metal and Li salt electrolyte in the coin cell configuration, the cell was disassembled, and the GO-S-0.1 after the contact was analyzed using XPS as shown in Figure S4. After contact, the surface of the GO-S-0.1 was partially reduced, and the majority of C-O and C=O functional groups were identified, confirming the preservation of GO surface properties. Additionally, the increased area of O-C=O is attributed to the solid electrolyte interface (SEI) layer formed with the electrolyte ions (Figure S4). The overall electrochemical behavior observed when applying GO-S-0.1 is schematically presented in Figure 4(d). The application of GO layers on PE-S can improve the ionic conductivity and provide high mechanical stability, ensuring that smooth and uniform Li dendrites are deposited onto the surface of the electrodes. However, when only PE-S is used, protruding and randomly distributed Li dendrites exist in the electrodes.

For practical application in Li-ion batteries, we further carried out an electrochemical test of GO-S-0.1 using asymmetric cells with lithium titanate (LTO) as the cathode and Li metal as the anode. Figure 5(a) displays the GCD curves of GO-S-0.1 at a current density of 100 mA g^{-1}. Based on the GCD results, cells with GO-S-0.1 exhibit relatively higher charge- and discharge-specific capacities than cells with PE-S. Figures 5(b) and 5(c) illustrate the rate capability test of GO-S-0.1 and PE at current densities ranging from 100 to 1000 mA g^{-1}. At a current density of 1000 mA g^{-1}, the retention of the charge storage capacities of GO-S-1 (69.7%) can reach a higher value than that of PE (66.4%). Moreover, we observed capacity degradation before and after thermal aging treatment in a conventional oven at 100°C for 1 h to confirm the thermal properties of GO-S-0.1. As shown in Figure 5(d), before undergoing thermal aging treatment, cells with GO-S-0.1 or PE-S exhibit a stable capacity retention rate at a current density of 100 mA g^{-1}. However, after aging treatment at 100°C for 1 h, a significant difference in cell performance was observed between GO-S-0.1 and PE-S. During the harsh thermal treatment process, cells with GO-S-0.1 can maintain their capacity up to 87%, whereas cells with PE-S retain only 13% of their initial capacity. These results can be attributed to the physical

damage and shrinkage of PE-S compared with GO-S-0.1, thereby demonstrating the unique stability performance of the GO coating layer on the PE membrane. Figures 5(e) and 5(f) also present the stability results from cells treated with GO-S-0.1 and PE-S. At a current density of 100 mA g^{-1}, cells with GO-S-0.1 exhibit a specific capacity value of 170 mAh g^{-1}, surpassing that of cells with PE-S. Furthermore, based on the GCD performance of GO-S-0.1, from the 1st to the 50th cycle, GO-S-0.1 maintains a stable voltage plateau region, which is consistent with the electrochemical stability results. Additionally, the cell configured as Li//LiFePO$_4$ (LFP) with the GO-S-0.1 separator was tested to demonstrate the applicability of GO-S-0.1. Figure S5a presents the galvanostatic charge-discharge (GCD) curve of Li//LFP at a current density of 100 mA g^{-1}. The cells incorporating the GO-S-0.1 and PE separators achieved initial capacitances of 140 mAh g^{-1} and 131 mAh g^{-1}, respectively. Moreover, regarding cycling stability, the cells containing GO-S-0.1 and PE demonstrate similar capacity retention for the first 50 cycles (Figure S5b). Additionally, the results of the thermal stability tests after 10 cycles are presented in Figure S5c. After undergoing thermal aging treatment at 100°C for 1 hour, the cell equipped with GO-S-0.1 retains 80% of its initial capacitance, whereas the cell with PE loses 80% of its initial capacitance. These test results, employing the LFP cathode, represent the superior separator properties of GO-S-0.1 in LIBs. The application of GO layers on the PE membrane enhances the overall mechanical and thermal stability, thereby ensuring high ionic conductivity and diffusion. These improvements contribute to the enhanced overall performance of the electrochemical cells.

4. Conclusions

The application of GO coating layers on a PE membrane in Li anode batteries provides numerous benefits. Fabrication allows for precise control over the thickness of the GO layers, leading to enhanced electrochemical and mechanical properties. The characterization results indicate that GO-S significantly improves the surface properties, thermal stability, wettability, and ionic conductivity of the separator material. The electrochemical performance of Li anode batteries using GO-S demonstrates exceptional stability and efficiency. In particular, GO-S-0.1 has superior cycling stability and the ability to maintain high charge- and discharge-specific capacities, even after extended cycling and harsh thermal aging. This remarkable performance is attributed to the reduction in dendrite growth and enhanced Li-ion diffusion facilitated by the GO layers. This study highlights the potential application of GO-coated PE separators in Li anode battery technology, providing improved safety, stability, and performance, which are crucial for the development of next-generation energy storage systems.

Data Availability

Access to data is restricted according to the policies of institutions and funding organization.

Conflicts of Interest

The authors declare that there is no conflict of interest regarding the publication of this paper.

Authors' Contributions

HeeYoung Lim was responsible for conceptualization, investigation, formal analysis, and writing of the original draft. Han Na Na was responsible for investigation and formal analysis. Eun Jung Jung was responsible for formal analysis. Wook Ahn was responsible for data curation. Jong Bae Park was responsible for data curation, writing, reviewing, and editing. John Hong was responsible for supervision, writing, reviewing, and editing. Young-Woo Lee was responsible for supervision, writing, reviewing, and editing.

Acknowledgments

Supplementary Materials

Figure S1: the cross-sectional SEM image of SEM image (a) PE-S, (b) GO-S-0.1, and (c) GO-S-0.5. Figure S2: chronoamperogram for (a) PE-S, (b) GO-S-0.1, and (c) GO-S-0.5 (inset images show Nyquist plots before and after the polarization experiment). Figure S3: (a) electrochemical performance of Li/GO-S-1/Li cell at a current density of $1\,mAh\,cm^{-2}$ for 600 h. (b) Li plating/striping curves of Li/GO-S-1/Li cell from 440 h to 450 h. Figure S4: XPS spectrum of C 1s for GO-S-0.1 after galvanostatic Li plating/stripping reaction. Figure S5: (a) galvanostatic charge-discharge curves of Li/PE/LFP and Li/GO-S-0.1/LFP cells at $100\,mA\,g^{-1}$. (b) Cycling performance of Li/PE/LFP and Li/GO-S-0.1/LFP cells at $100\,mA\,g^{-1}$. (c) Thermal test of Li/PE/LFP and Li/GO-S-0.1/LFP cells after 100°C, 1 h aging. (Supplementary Materials)

References

[1] S. Choi and G. Wang, "Advanced lithium-ion batteries for practical applications: technology, development, and future perspectives," *Advanced Materials Technologies*, vol. 3, no. 9, article 1700376, 2018.

[2] B. Diouf and R. Pode, "Potential of lithium-ion batteries in renewable energy," *Renewable Energy*, vol. 76, pp. 375–380, 2015.

[3] A. Väyrynen and J. Salminen, "Lithium ion battery production," *The Journal of Chemistry Thermodynamics*, vol. 46, pp. 80–85, 2012.

[4] C. M. Costa and S. Lanceros-Mendez, "Recent advances on battery separators based on poly (vinylidene fluoride) and its copolymers for lithium-ion battery applications," *Current Opinion in Electrochemistry*, vol. 29, article 100752, 2021.

[5] P. Ragupathy, S. D. Bhat, and N. Kalaiselvi, "Electrochemical energy storage and conversion: an overview," *Wiley Interdisciplinary Reviews: Energy and Environment*, vol. 12, no. 2, article e464, 2023.

[6] B. Scrosati, J. Hassoun, and Y. K. Sun, "Lithium-ion batteries. A look into the future," *Energy & Environmental Science*, vol. 4, no. 9, pp. 3287–3295, 2011.

[7] S. S. Liang, W. Yan, X. Wu et al., "Gel polymer electrolytes for lithium ion batteries: fabrication, characterization and performance," *Solid State Ionics*, vol. 318, pp. 2–18, 2018.

[8] R. Li, J. Li, L. X. Li et al., "A bifunctional composite artificial solid electrolyte interphase for high stable solid-state lithium batteries," *Colloids and Surfaces A: Physicochemical and Engineering Aspects*, vol. 657, article 130600, 2023.

[9] N. Nitta, F. Wu, J. T. Lee, and G. Yushin, "Li-ion battery materials: present and future," *Materials Today*, vol. 18, no. 5, pp. 252–264, 2015.

[10] P. Guan, L. Zhou, Z. Yu et al., "Recent progress of surface coating on cathode materials for high-performance lithium-ion batteries," *Journal of Energy Chemistry*, vol. 43, pp. 220–235, 2020.

[11] Z. Zou, Z. Hu, and H. Pu, "Lithium-ion battery separators based-on nanolayer co-extrusion prepared polypropylene nanobelts reinforced cellulose," *Journal of Membrane Science*, vol. 666, article 121120, 2023.

[12] G. Zubi, R. Dufo-López, M. Carvalho, and G. Pasaoglu, "The lithium-ion battery: state of the art and future perspectives," *Renewable and Sustainable Energy Reviews*, vol. 89, pp. 292–308, 2018.

[13] K. Liu, Y. Liu, D. Lin, A. Pei, and Y. Cui, "Materials for lithium-ion battery safety," *Science Advances*, vol. 4, no. 6, article eaas9820, 2018.

[14] L. Zhao, J. Fu, Z. du et al., "High-strength and flexible cellulose/PEG based gel polymer electrolyte with high performance for lithium ion batteries," *Journal of Membrane Science*, vol. 593, article 117428, 2020.

[15] G. Wei, R. Huang, G. Zhang et al., "A comprehensive insight into the thermal runaway issues in the view of lithium-ion battery intrinsic safety performance and venting gas explosion hazards," *Applied Energy*, vol. 349, article 121651, 2023.

[16] M. Ravi, S. Song, J. Wang, T. Wang, and R. Nadimicherla, "Ionic liquid incorporated biodegradable gel polymer electrolyte for lithium ion battery applications," *Journal of Materials Science: Materials in Electronics*, vol. 27, no. 2, pp. 1370–1377, 2016.

[17] Z. Qian, Y. Li, and Z. Rao, "Thermal performance of lithium-ion battery thermal management system by using mini-channel cooling," *Energy Conversion and Management*, vol. 126, pp. 622–631, 2016.

[18] Q. Liu, R. Liu, Y. Cui et al., "Dendrite-free and long-cycling lithium metal battery enabled by ultrathin, 2D shield-defensive, and single lithium-ion conducting polymeric membrane," *Advanced Materials*, vol. 34, no. 33, 2022.

[19] X. Shen, H. Liu, X. B. Cheng, C. Yan, and J. Q. Huang, "Beyond lithium ion batteries: higher energy density battery systems based on lithium metal anodes," *Energy Storage Materials*, vol. 12, pp. 161–175, 2018.

[20] S. Xia, J. Lopez, C. Liang et al., "High-rate and large-capacity lithium metal anode enabled by volume conformal and self-healable composite polymer electrolyte," *Advanced Science*, vol. 6, no. 9, article 1802353, 2019.

[21] X. Zhu, X. Jiang, X. Ai, H. Yang, and Y. Cao, "A highly thermo-stable ceramic-grafted microporous polyethylene separator for safer lithium-ion batteries," *ACS Applied Materials & Interfaces*, vol. 7, no. 43, pp. 24119–24126, 2015.

[22] K. Prasanna, C. S. Kim, and C. W. Lee, "Effect of SiO_2 coating on polyethylene separator with different stretching ratios for application in lithium ion batteries," *Materials Chemistry and Physics*, vol. 146, no. 3, pp. 545–550, 2014.

[23] K. J. Kim, Y. H. Kim, J. H. Song, Y. N. Jo, J. S. Kim, and Y. J. Kim, "Effect of gamma ray irradiation on thermal and electrochemical properties of polyethylene separator for Li ion batteries," *Journal of Power Sources*, vol. 195, no. 18, pp. 6075–6080, 2010.

[24] Y. K. Kim, W. Y. Lee, K. J. Kim, J. S. Yu, and Y. J. Kim, "Shutdown-functionalized nonwoven separator with improved thermal and electrochemical properties for lithium-ion batteries," *Journal of Power Sources*, vol. 305, pp. 225–232, 2016.

[25] K. J. Kim, M. S. Park, T. Yim, J. S. Yu, and Y. J. Kim, "Electron-beam-irradiated polyethylene membrane with improved electrochemical and thermal properties for lithium-ion batteries," *Journal of Applied Electrochemistry*, vol. 44, no. 3, pp. 345–352, 2014.

[26] Y.-J. Kim, H.-S. Kim, C.-H. Doh, S.-H. Kim, and S.-M. Lee, "Technological potential and issues of polyacrylonitrile based nanofiber non-woven separator for Li-ion rechargeable batteries," *Journal of Power Sources*, vol. 244, pp. 196–206, 2013.

[27] L. Tan, Y. Sun, C. Wei et al., "Design of robust, lithiophilic, and flexible inorganic-polymer protective layer by separator engineering enables dendrite-free lithium metal batteries with $LiNi_{0.8}Mn_{0.1}Co_{0.1}O_2$ Cathode," *Small*, vol. 17, no. 13, article e2007717, 2021.

[28] N. Sharma, S. Tomar, M. Shkir, R. Kant Choubey, and A. Singh, "Study of optical and electrical properties of graphene oxide," *Materials Today: Proceedings*, vol. 36, pp. 730–735, 2021.

[29] H. Park, S. Lim, D. D. Nguyen, and J. W. Suk, "Electrical measurements of thermally reduced graphene oxide powders under pressure," *Nanomaterials*, vol. 9, no. 10, p. 1387, 2019.

[30] A. T. Smith, A. M. LaChance, S. Zeng, B. Liu, and L. Sun, "Synthesis, properties, and applications of graphene oxide/reduced graphene oxide and their nanocomposites," *Nano Materials Science*, vol. 1, no. 1, pp. 31–47, 2019.

[31] G. G. Politano and C. Versace, "Electrical and optical characterization of graphene oxide and reduced graphene oxide thin films," *Crystals*, vol. 12, no. 9, p. 1312, 2022.

[32] G. Jiang, K. Li, J. Mao et al., "Sandwich-like prussian blue/graphene oxide composite films as ion-sieves for fast and uniform Li ionic flux in highly stable Li metal batteries," *Chemical Engineering Journal*, vol. 385, article 123398, 2020.

[33] V. Jabbari, V. Yurkiv, A. Ghorbani, F. Mashayek, and R. Shahbazian-Yassar, "Fast rate lithium metal batteries with long lifespan enabled by graphene oxide confinement," *Energy Advances*, vol. 2, no. 5, pp. 712–724, 2023.

[34] J. Zhu, C. Chen, Y. Lu et al., "Highly porous polyacrylonitrile/graphene oxide membrane separator exhibiting excellent anti-self-discharge feature for high-performance lithium–sulfur batteries," *Carbon*, vol. 101, pp. 272–280, 2016.

[35] W. Ren, Y. Zheng, Z. Cui, Y. Tao, B. Li, and W. Wang, "Recent progress of functional separators in dendrite inhibition for lithium metal batteries," *Energy Storage Materials*, vol. 35, pp. 157–168, 2021.

[36] Z. Yan, C. Zhou, C. Li et al., "Li_3N film modified separator with homogenization effect of lithium ions for stable lithium metal battery," *Progress in Natural Science: Materials International*, vol. 31, no. 6, pp. 845–851, 2021.

[37] Y. Chen, J. Li, Y. Ju et al., "Regulating Li-ion flux distribution via holey graphene oxide functionalized separator for dendrite-inhibited lithium metal battery," *Applied Surface Science*, vol. 592, article 153222, 2022.

[38] X. Yin, W. Deng, X. Zhou et al., "Revealing anion adsorption mechanism for coating layer on separator toward practical Li metal batteries," *ACS Applied Materials & Interfaces*, vol. 13, no. 20, pp. 23584–23591, 2021.

[39] G. Zhu, X. Jing, D. Chen, and W. He, "Novel composite separator for high power density lithium-ion battery," *International Journal of Hydrogen Energy*, vol. 45, no. 4, pp. 2917–2924, 2020.

[40] X. Liu, K. Song, C. Lu et al., "Electrospun PU@ GO separators for advanced lithium ion batteries," *Journal of Membrane Science*, vol. 555, pp. 1–6, 2018.

[41] K. Song, Y. Huang, X. Liu, Y. Jiang, P. Zhang, and Y. Ding, "Electrospun PI@ GO separators for Li-ion batteries: a possible solution for high-temperature operation," *Journal of Sol-Gel Science and Technology*, vol. 94, no. 1, pp. 109–117, 2020.

[42] H. Liao, H. Zhang, G. Qin, Z. Li, L. Li, and H. Hong, "A macroporous graphene oxide-based membrane as a separator with enhanced thermal stability for high-safety lithium-ion batteries," *RSC Advances*, vol. 7, no. 36, pp. 22112–22120, 2017.

[43] D. H. Kusumawati and T. N. Agustin, "Characteristic of nanofiber PVA-graphene oxide (GO) as lithium battery separator," *Journal of Physics: Conference Series*, vol. 2623, no. 1, article 012008, 2023.

[44] Z. Huang, W. Sun, Z. Sun, R. Ding, and X. Wang, "Graphene-based materials for the separator functionalization of lithium-ion/metal/sulfur batteries," *Materials*, vol. 16, no. 12, p. 4449, 2023.

[45] J. Cui, J. Liu, C. He, J. Li, and X. Wu, "Composite of polyvinylidene fluoride-cellulose acetate with Al $(OH)_3$ as a separator for high-performance lithium ion battery," *Journal of Membrane Science*, vol. 541, pp. 661–667, 2017.

[46] Q. Liu, Y. Liu, X. Jiao et al., "Enhanced ionic conductivity and interface stability of hybrid solid-state polymer electrolyte for rechargeable lithium metal batteries," *Energy Storage Materials*, vol. 23, pp. 105–111, 2019.

[47] S. Alipoori, M. M. Torkzadeh, M. H. M. Moghadam, S. Mazinani, S. H. Aboutalebi, and F. Sharif, "Graphene oxide: an effective ionic conductivity promoter for phosphoric acid-doped poly (vinyl alcohol) gel electrolytes," *Polymer*, vol. 184, article 121908, 2019.

[48] Y. Jiang, C. Xu, K. Xu et al., "Surface modification and structure constructing for improving the lithium ion transport properties of PVDF based solid electrolytes," *Chemical Engineering Journal*, vol. 442, article 136245, 2022.

[49] D. Zhang, L. Ding, T. Wu et al., "Facile preparation of a lithium-ion battery separator with thermal shutdown function based on polypropylene/polyethylene microsphere composites," *Industrial & Engineering Chemistry Research*, vol. 60, no. 50, pp. 18530–18539, 2021.

[50] S. Ramanathan, S. Moorthy, S. Ramasundaram et al., "Grape seed extract assisted synthesis of dual-functional anatase TiO_2 decorated reduced graphene oxide composite for supercapacitor electrode material and visible light photocatalytic degradation of bromophenol blue dye," *ACS Omega*, vol. 6, no. 23, pp. 14734–14747, 2021.

[51] K. N. Kudin, B. Ozbas, H. C. Schniepp, R. K. Prud'homme, I. A. Aksay, and R. Car, "Raman spectra of graphite oxide and functionalized graphene sheets," *Nano Letters*, vol. 8, no. 1, pp. 36–41, 2008.

[52] H. Ahmad, M. Fan, and D. Hui, "Graphene oxide incorporated functional materials: a review," *Composites Part B: Engineering*, vol. 145, pp. 270–280, 2018.

[53] F. T. Johra, J. W. Lee, and W. G. Jung, "Facile and safe graphene preparation on solution based platform," *Journal of Industrial and Engineering Chemistry*, vol. 20, no. 5, pp. 2883–2887, 2014.

[54] Y. Yoon, H. Kye, W. S. Yang, and J. W. Kang, "Comparing graphene oxide and reduced graphene oxide as blending materials for polysulfone and polyvinylidene difluoride membranes," *Applied Sciences*, vol. 10, no. 6, p. 2015, 2020.